Weldability and Microstructure of a Titanium Aluminide

Cooling rate has a profound effect on the microstructure and properties of titanium aluminide welds

BY S. A. DAVID, J. A. HORTON, G. M. GOODWIN, D. H. PHILLIPS AND R. W. REED

ABSTRACT. Full-penetration gas tungsten arc (GTA) and electron beam (EB) welds were made on a modified titanium aluminide (Ti-14 wt-% Al-21 wt-% Nb). Welding speeds ranged from 2.1 to 42 mm/s (5 to 100 in./min).

The alloy showed no evidence of hot cracking and had a measured Sigmajig threshold stress of greater than 240 MPa (35 ksi). This value is within the range of 69–345 MPa (10–50 ksi) for crack-resistant austenitic stainless steels and some of the crack-resistant nickel aluminides. Electron beam weld microstructural features were found to be a strong function of welding speed and energy input, and thus the cooling rate. The fusion zone (FZ) microstructure of EB welds contained predominantly fine, acicular ordered α_2 phase at low welding speeds, and predominantly retained β (metastable) at high welding speeds. In the heat-affected zone (HAZ) there was a gradual variation in microstructure from ordered, acicular α_2 near the fusion line to $\alpha_2 + \beta$ in the far HAZ. Microhardness profiles across the weldment indicated the hardness in the HAZ and FZ to be much higher than the base metal (BM) in all welds. The hardness profiles across the HAZ and FZ were more uniform in welds made at low welding speeds than at high welding speeds. The hardness profile across the welds made at higher welding speeds showed a decrease in the weld centerline hardness relative to those made at lower welding speeds. This may be attributed to retention of metastable β phase.

Finally, Gleeble hot-ductility testing revealed the presence of a ductility dip during the heating portion of the weld thermal cycle. However, no ductility dip was observed during cooling.

Introduction

In recent years, considerable interest has developed in the ordered intermetallic compounds because of unique properties that make them potential candidates for high-temperature structural applications. Weldability is a key issue in the development of these alloys because joining by conventional welding processes is an important means of fabricating engineering alloys into structural components. Earlier welding studies have concentrated on ordered alloys that have $L1_2$-type cubic stacking character (Refs. 1–5). These alloys include boron-doped Ni_3Al, $(Fe, Co)_3V$ and $(Fe, Ni)_3V$ types. Such ordered alloys are ductile with tensile elongations exceeding 35%.

Another alloy that has been gaining considerable attention is the α_2 titanium aluminide that is being developed as a structural material for aerospace applications (Refs. 6–8). The intermetallic compound Ti_3Al, also referred to as α_2, has an ordered DO_{19}-type lattice structure. Although this ordered intermetallic alloy is lighter and stiffer than conventional titanium alloys, its major shortcoming is limited ductility at room temperature. Earlier investigation has shown that ternary and quaternary additions of β (bcc) stabilizing elements such as Nb, V, Mo and W can significantly increase the ductility of this alloy primarily through reduction in slip lengths and ordering kinetics. Furthermore, recent studies have also developed a new family of Ti alloys based roughly on the composition Ti_3Al with ternary additions of Nb (Refs. 9, 10). In these alloys, it is possible through rapid cooling to suppress β decomposition to α_2, and instead promote the formation of an ordered, metastable bcc β superlattice structure (CsCl), also referred to as B2, over a wide range of alloy compositions. An alloy of practical significance is Ti-14 wt-% Al-21 wt-% Nb (Ti-14-21).

An area of interest that lacks information is the weldability of this alloy. Limited weldability studies have shown that moderate cooling rates associated with conventional arc welding processes promote the formation of a fine acicular α_2 structure with almost zero ductility. Several investigations are under way to characterize laser and gas tungsten arc welds (Refs. 11, 12). This paper describes the weldability of Ti-14-21 using GTA and EB welding processes. Also, it identifies factors controlling the weldability and microstructural features.

KEY WORDS

Titanium Aluminide
Aluminide Microstructure
Aluminide Weldability
Aluminide Microhardness
Gleeble Testing
Sigmajig Testing
Intermetallics
Ordered Intermetallics
Alpha 2 Ti Aluminide
GTA/EB Welding

Experimental Procedure

Autogenous GTA and EB welds were made on 5 × 5 × 0.6 cm (2 × 2 × 0.25 in.) coupons of Ti-13.5 wt-% Al-21.5 wt-% Nb (Ti-24 at.-% Al-11 at.-% Nb) alloy obtained from hot-rolled plate. Gas tungsten arc welds were made at speeds ranging from 2.1 to 8.4 mm/s (5 to 20 in./min) and EB welds were made at speeds ranging from 2.1 to 42 mm/s (5 to 100 in./min). Welds were made at different welding speeds in order to vary the heat input and hence the cooling rate. Welding parameters used are listed in Table 1. The sensitivity to fusion zone hot-cracking of this alloy was established using the Sigmajig weldability test described elsewhere (Ref. 13). The test ranks materials by quantitatively measuring a threshold stress above which cracking occurs.

Differential thermal analysis (DTA) was carried out in helium in a Mettler ther-

S. A. DAVID, J. A. HORTON, G. M. GOODWIN and R. W. REED are with the Metals and Ceramics Div., Oak Ridge National Laboratory, Oak Ridge, Tenn. D. H. PHILLIPS is with GE Aircraft Engines, Cincinnati, Ohio.

Table 1—Welding Parameters

GTA Welds	Current A	Voltage V	Speed mm/s	Heat Input[(a)] J/mm
TA-4	200	14	2.1	1000
TA-5	200	14	4.2	500
TA-6	200	14	8.4	250
EB Welds	**Current mA**	**Voltage kV**	**Speed mm/s**	**Heat input[(a)] J/mm**
TA-7	6.5	150	2.1	370
TA-13	10.0	150	12.5	96
TA-14	14.1	150	25.0	67
TA-15	19.0	150	42.0	54

(a) Assumed efficiencies: GTAW 75% (Ref. 22); EBW, 80% (Ref. 23).

moanalyzer. A sample weighing approximately 7 to 8 g was heated to about 50°C (90°F) above the presumed β transus temperature of the sample and then cooled at a constant rate of 10°C/min (18°F/min). During cooling, a 12-channel compensated recorder traced DTA curves.

Hot-ductility testing was performed in vacuum using a Gleeble 1500 thermomechanical simulator. Since the availability of this alloy was limited, subsize specimens were used. The specimen geometry and the procedure for testing were as described by Santella, *et al* (Ref. 3).

Sections of the welds were prepared for metallographic analysis by standard metallographic techniques. The specimens were etched with Kroll's reagent (1 to 3 mL HF, 4 to 6 mL HNO_3 and 100 mL H_2O). DPH microhardness traverses were made across the welds using a Shimadzu microhardness tester with a 500-g load. Specimens for transmission electron microscopy (TEM) were prepared by spark discharge machining of 3-mm disks from the weldments at different locations, *i.e.*, heat-affected zone (HAZ), fusion zone (FZ) and base metal (BM), followed by electropolishing of the disks in an electrolyte (600 parts methanol, 360 parts butyl cellusolve and 60 parts perchloric acid) at −15°C and 40 V, and a current of 160 mA. Transmission electron microscopy examinations were conducted using a Philips EM430 microscope.

Results and Discussion

GTA and EB Welding

Autogenous GTA and EB welds were produced in the Nb-modified Ti_3Al alloy (Ti-14-21) without cracking. It was difficult to produce full-penetration welds using the GTA welding process. Top surface and transverse sections of the autogenous welds made on 6-mm (0.25-in.) thick plate are shown in Fig. 1. The welds made using the GTA welding process tended to be wide and shallow—Figs. 1A and 1B. The weld pool shape and the shallow weld penetration suggest that the controlling mechanism for the development of the weld pool is convective heat transfer resulting from a radially outward flow of molten metal. An outward flow, from the center of the pool to the periphery, would transfer the heat to the lateral face of the weld bead more efficiently. This combined with the relatively low thermal diffusivity of the alloy would promote the shallow weld bead geometry. This was also consistent with other welds made at lower welding speeds, that resulted in weld beads of increased width with minimal increase in penetration. The increased energy input (per unit area), due to the decreased travel speed, apparently was once again transported radially outward by the molten metal, thereby increasing the width of the weld bead considerably more than the depth of penetration. However, it should be pointed out that successful full-penetration GTA welds were obtained using 0.7-mm (0.03-in.) thick specimens. In contrast to the limited penetration of GTA welds on thick sections (6 mm), full-penetration welds were readily obtained using the EB welding process—Figs. 1C and 1D.

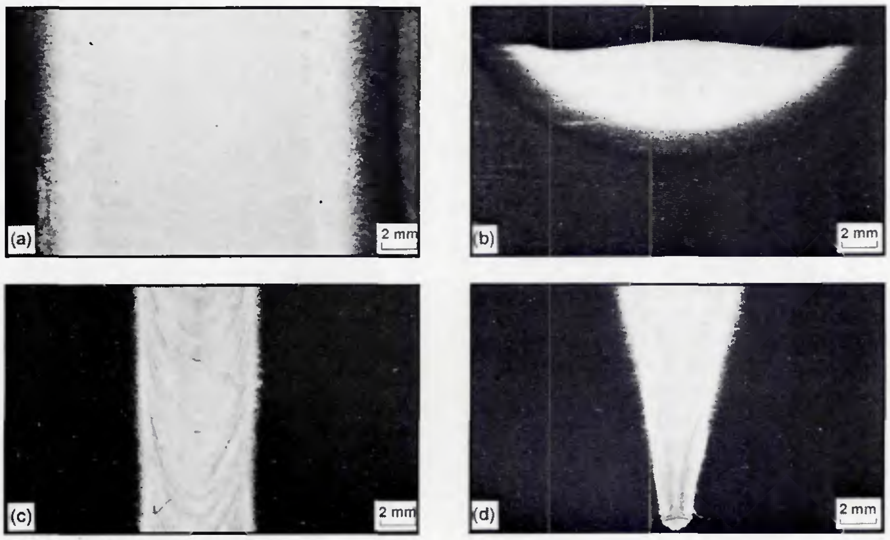

Fig. 1—Optical photomicrograph showing surface and transverse sections. A and B—GTA weld TA-4; C and D—EB weld TA-7.

Sigmajig Weldability Test

Generally, the susceptibility to FZ solidification cracking and HAZ cracking may be established using any one of several conventional hot-cracking tests (Ref. 14). However, most of these tests are only applicable to thicknesses greater than 1.5 mm (0.06 in.). Since the penetration obtained in thick sections of Ti-14-21 alloy during GTA welding is inadequate to evaluate the hot-cracking (solidification cracking) susceptibility of this alloy, a recently developed hot-cracking test (Sigmajig) that uses thin sheet material was used. The test evaluates the hot-cracking tendency of the alloy, often using the GTA welding process.

In the Sigmajig test, an indicator that is used to determine the susceptibility to fusion zone cracking is the threshold stress, σ_0, above which cracking first occurs during welding. Sigmajig tests were performed using the GTA welding process on 0.7-mm-thick (0.03-in.) sheet using 65 A DCEN, 14.5 mm/s (35 in./min) travel, and 0.9-mm (0.035-in.) arc length. Test results for the alloy are summarized in Fig. 2. The welds were resistant to hot-crack initiation at the highest stress investigated, 240 MPa (35 ksi), and thus have a threshold stress σ_0, greater than 240 MPa (35 ksi). This lower bound value is within the material range of austenitic stainless steels 103–345 MPa (15–50 ksi) and some of the crack-resistant nickel aluminides (Ni_3Al) as shown in Fig. 2. In this figure, the data for the stainless steels and the nickel aluminides represent the extreme values of threshold cracking stress measured on several heats of material. They reflect variations within the nominal composition due to minor element effects, fabrication history, etc. Comparison of threshold cracking values among various classes of alloys is uncertain on a quantitative basis, particularly with only one heat of the material in question. Qualitatively, however, this result indicates excellent resistance to hot-cracking for the Nb-modified Ti_3Al. In addition, it should be mentioned that the alloy showed no HAZ cracking. Heat-affected zone cracking has been a severe problem in some of the other ductile aluminides such as Ni_3Al (Ref. 1).

Although the alloy showed excellent resistance to solidification cracking, the test coupons showed a tendency to solid-state cracking well below the solidification temperature in a very brittle fashion during cooling subsequent to the test. Scanning electron microscopy (SEM) examination of the crack surface revealed predominantly cleavage-type failure in the FZ, a mixed mode of cleavage and ductile failure in the HAZ, and ductile (typical of titanium alloys) failure in the base metal. An SEM micrograph of the fractured surface is shown in Fig. 3. The reason for this unusual cracking behavior during cooling of this alloy may be related to the solid-state phase transformation that occurs in the FZ and the HAZ that experiences temperatures in excess of the β transus. It is well established that at moderate cooling rates from elevated temperatures, the alloy transforms from β to brittle acicular α_2. The observed brittle failure of the weld during cooling is also consistent with previous research that has shown that Ti_3Al exhibits a high ductile-brittle transition temperature (Ref. 8). In addition, since the Sigmajig test was performed in open atmosphere (albeit with adequate inert gas shielding during welding), the potential for oxygen contamination existed especially in the fusion zone. In titanium alloys, oxygen contamination has been found to lower ductility (Refs. 15, 16). In the Nb-modified Ti_3Al, it has been found that oxygen levels greater than 1000 ppm dramatically decrease room-temperature ductility (Ref. 17). These factors, combined with thermal and residual stresses, may be the cause for the observed solid-state cracking. It should be noted that the above observed cracking phenomenon was unique to the Sigmajig test specimens only. Such solid-state cracking was not observed in any of the full-penetration electron beam welds, or thick- section partial-penetration GTA welds.

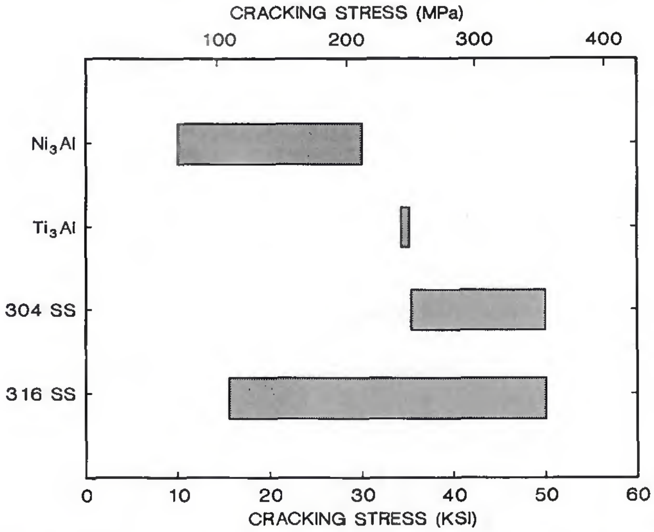

Fig. 2—Experimentally measured Sigmajig test cracking stress for various alloys.

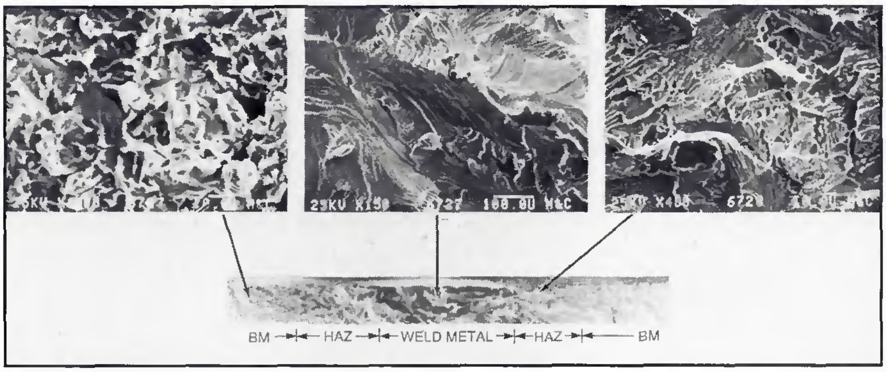

Fig. 3—SEM photomicrograph showing fracture mode in various regions of the GTA weld that cracked during cooling in the Sigmajig test.

Microstructure

Since full-penetration welds were not obtained in thick sections (6 mm) using GTA welding process, detailed microstructural characterization of the GTA welds was not performed. The extensive microstructural characterization described in this section refers to only electron beam welds made on 6-mm-thick specimens.

The microconstituents and microstructural features of Ti-14-21 alloy weldments may be understood better with the aid of a pseudo-binary diagram of the Ti_3Al-Nb system proposed by several investigators (Refs. 18, 19). Figure 4 shows the Ti_3Al-Nb system with varying percentages of Nb. The composition of interest is Ti-14-21. From the phase diagram, it is evident that alloys containing less than 5 wt-% Nb when rapidly cooled from the bcc β phase field, transform martensitically to the hcp α' phase during rapid cooling (Refs. 10, 20). However, in alloys richer in Nb the M_s temperature is well-below room temperature, thus increasing the stability of β to allow for the development of α_2/β microstructures. Depending on the process-

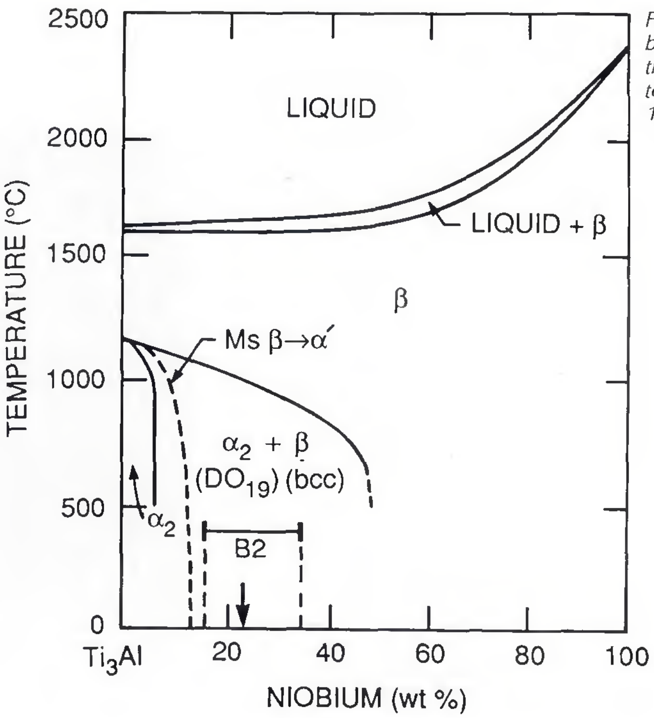

Fig. 4—Pseudo-binary diagram of the Ti_3Al + Nb system (Refs. 10, 18, 19).

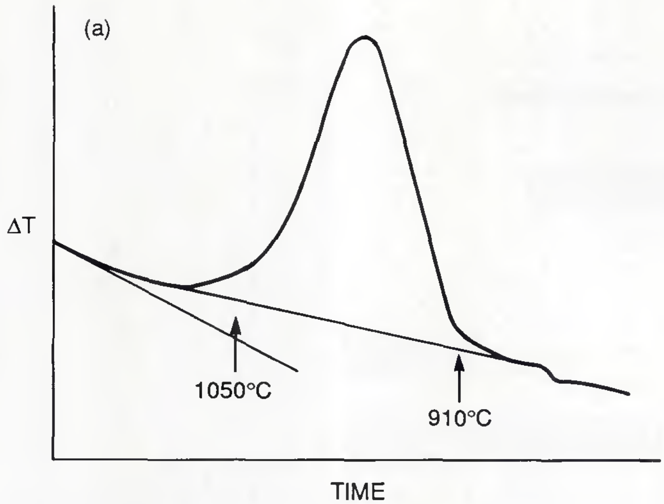

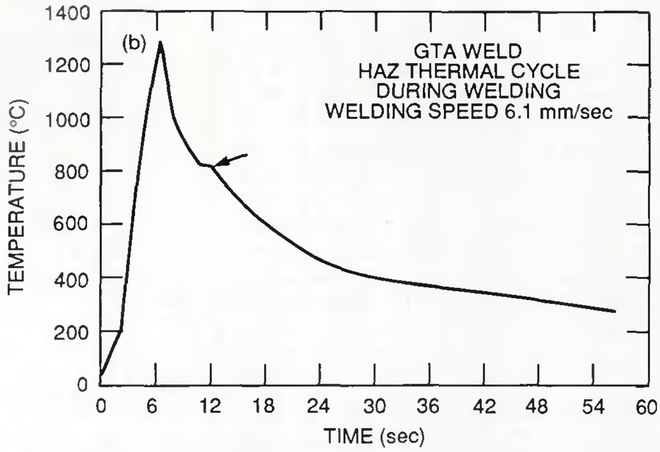

Fig. 5 — A — Differential thermal analysis (DTA) trace of Ti-14-21 alloy; B — HAZ thermal cycle during GTA welding.

ing conditions, in particular the cooling rate, it is possible to retain either disordered β or ordered metastable β designated as B2. Formation of a ω-type phase in the β-phase matrix, subsequent to ordering, may also occur (Ref. 10).

A DTA trace at 10°C/min for Ti-14-21 shown in Fig. 5A reveals the decomposition of high-temperature bcc phase (β) to a low-temperature hcp phase at 1050°C (1922°F). This temperature corresponds to conditions approaching equilibrium cooling. Whether this transformation occurs directly from β to an ordered hcp (α_2) or whether it first occurs to form a disordered hcp (α) phase which subsequently orders, was not determined in this investigation. However, this temperature may vary depending on the cooling rate. Figure 5B shows a typical weld thermal cycle experienced by the alloy in the HAZ close to the fusion line during GTA welding. Unlike the DTA curve shown in Fig. 5A, the free-cooling portion of the thermal cycle shows a sharp break on the curve indicating the bcc-to-hcp phase transformation start temperature of 830°C (1526°F). The break on the curve at 830°C was consistently reproducible for the same welding conditions. This observed transformation temperature was much lower than the equilibrium β transus temperature due to a higher cooling rate encountered during weld thermal cycle. An increase in cooling rate has been found to decrease the transformation start temperature considerably in both conventional Ti alloys and α_2 titanium aluminides (Ref. 12).

Base Metal

Figure 6 shows the microstructural features of the α/β base metal. The microstructure consists predominantly of ordered α_2 with small islands of Nb-rich β phase at α_2 grain boundaries. Figure 7 shows a TEM micrograph of the base metal showing a directionally oriented structure comprised of an α_2 matrix surrounding β phase. The β is a disordered bcc phase. EDS analysis showed that the β phase contained about 30 wt-% Nb and 11 wt-% Al, while the matrix α_2 phase contained about 20 wt-% Nb and 16 wt-% Al. The Ti content of the β phase was about 5 wt-% less than that of the matrix phase (Table 2).

Weld Metal

Figure 8 shows columnar β grains growing epitaxially from the near HAZ into the FZ of the EB weld produced at 2.1 mm/s (5 in./min). A distinct line, marked by the arrows, separates the FZ from the HAZ.

Table 2—Phase Analysis of the Base Metal

	(wt-%)		
	Al	Nb	Ti
α_2-phase	16.0	19.6	64.4
β-phase	10.6	29.6	59.8
Nominal	13.5	21.5	65.0

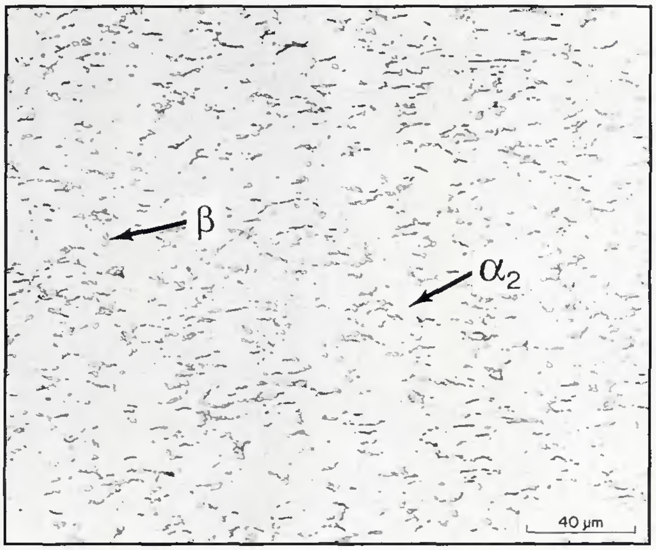

Fig. 6 — Photomicrograph showing typical base metal microstructure.

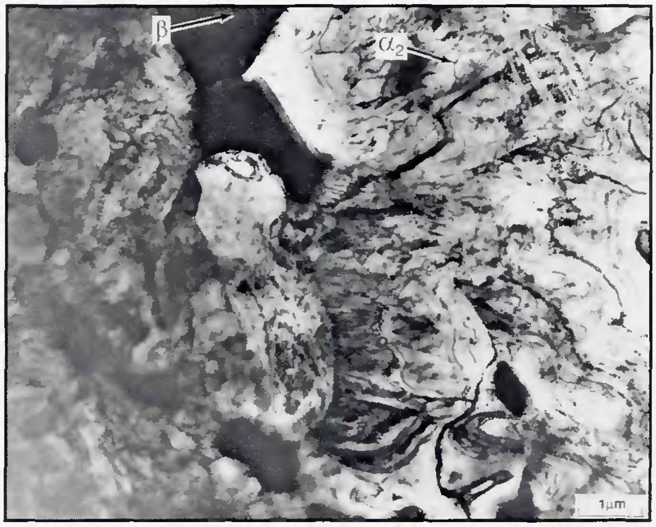

Fig. 7 — Bright field TEM micrograph of the as-received wrought Alloy Ti-14-21.

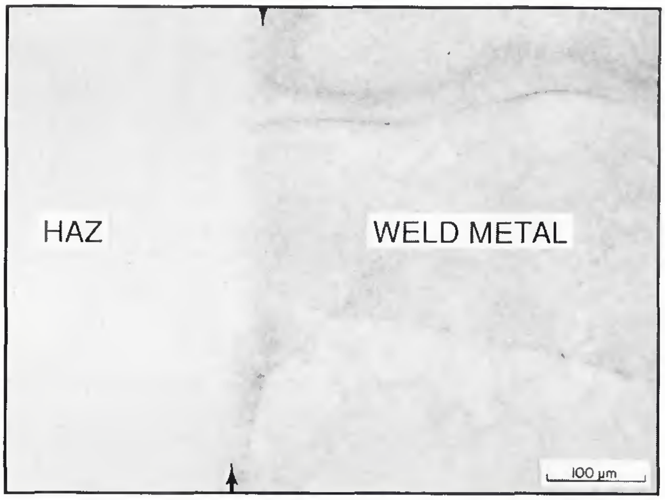

Fig. 8 — Photomicrograph of an EB weld showing both FZ and the HAZ microstructures. Arrow indicates fusion line.

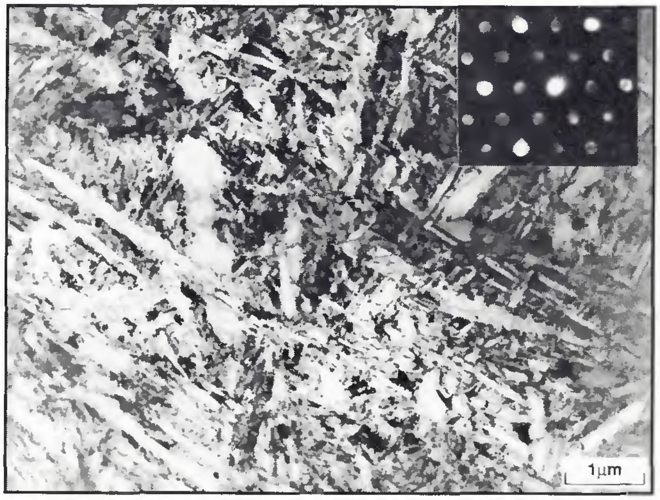

Fig. 9 — Bright-field TEM micrograph of the EB weld FZ (welding speed 2.1 mm/s).

To a large extent the solidification substructure was masked by the transformation of β solid solution to ordered acicular α_2. Also, the optical microscopy of the fusion zone revealed no significant variations in the microstructure with varying welding speed, with all specimens exhibiting distinct, acicular needles of α_2. However, TEM examination of the FZ revealed significant variations in the microstructure with an increase in welding speed, and thus the cooling rate. Specimens were examined by TEM after EB welding at speeds 2.1, 12.5 and 25 mm/s (5, 30 and 60 in./min). Corresponding heat inputs for the EB welds were estimated to be 370, 96 and 67 J/mm. A wide range of microstructures and phases was present. In the weld made at 2.1 mm/s with high heat input, 370 J/mm, and thus low cooling rate, the structure was predominantly acicular α_2 — Fig. 9. This microstructure also corresponded to the highest hardness measured of the three different welds made at three different speeds and heat inputs.

In welds made at 12.5 mm/s, with a heat input of 96 J/mm, the cooling rate appears to be fast enough to largely suppress the β to α_2 phase transformation and yield a microstructure containing predominantly metastable β (B2) as shown in Fig. 10A. The needles in Fig. 10A are thin, probably martensitically formed, platelets. The [100] diffraction pattern in Fig. 10A shows the extra reflections that arise from the needles. Figure 10B is a dark-field micrograph illuminating the needles. Diffraction analysis indicated that the needle structure could be considered as a 4% distortion of the α_2 structure or could be considered as a 4% distortion of the ω structure. It appears to be somewhat analogous to the α'' orthorhombic distortion of the β-Ti phase. The structure of these phases after rapid cooling of similar alloys was previously described by Strychor, *et al.* (Ref. 10).

Microstructures of welds made at 25 mm/s with a low heat input of 67 J/mm appeared similar to the 12.5 mm/s welds. The structure was predominantly metastable β (B2); however, the B2 reflections were weak.

Microprobe analysis was performed across several dendrites revealed by a combination of mechanical polishing and chemical etching. Microprobe traces across several dendrites for welds made at two different speeds revealed no significant segregation of either Al or Nb — Fig. 11. Also, the Al content of the FZ was same as that of the BM, indicating no loss of Al during EB welding.

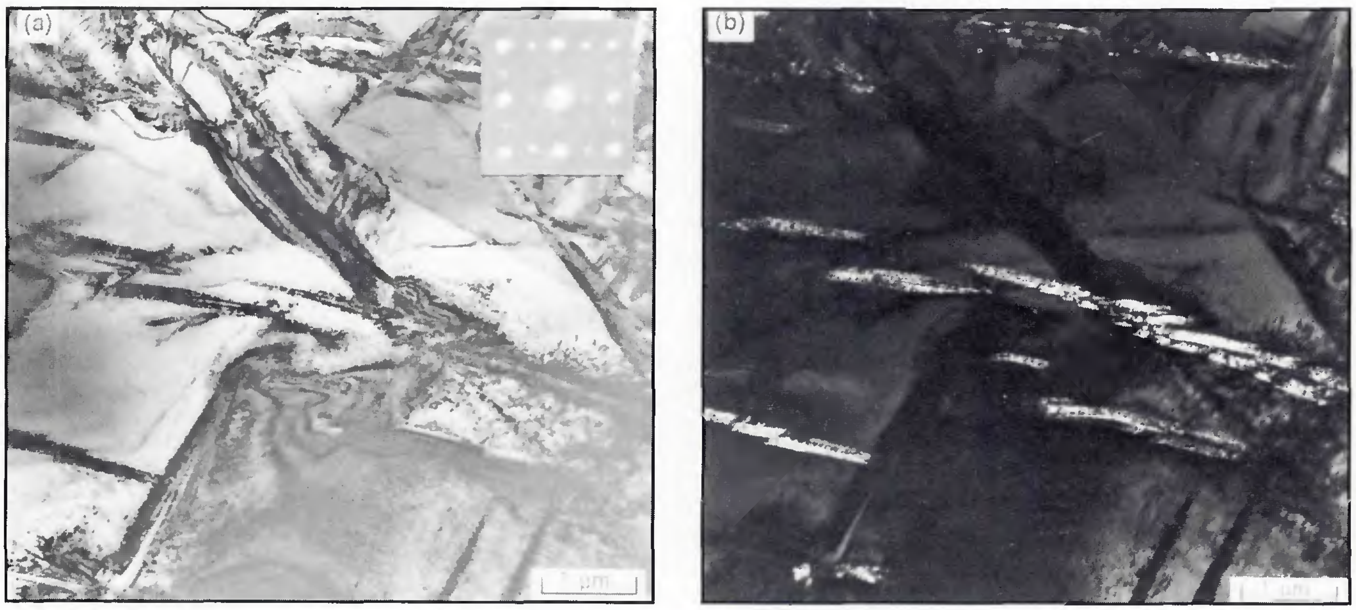

Fig. 10 — A — Bright-field; B — dark-field TEM micrograph of EB weld FZ (welding speed 12.5 mm/s).

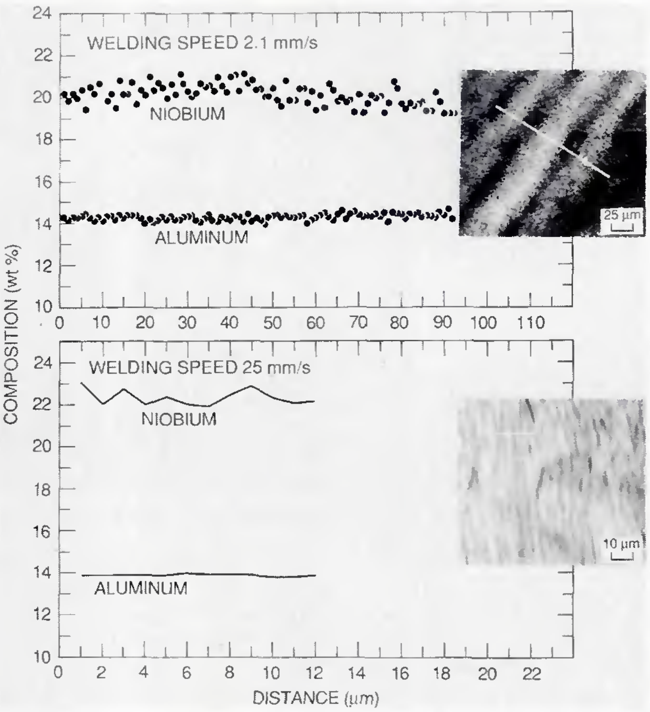

Fig. 11—Electron probe microanalysis trace on weld metal for two EB welds in Ti-14-21 made at 2.1 mm/s and 25 mm/s.

Heat-Affected Zone

The microstructural features across the HAZ varied in accordance with the phase diagram and the peak temperatures reached in the HAZ. Variations in the microstructure across the HAZ for a high energy input EB weld made at 2.1 mm/s (5 in./min) are shown in Fig. 12. Part of the HAZ that experienced temperatures in excess of the β transus (near the fusion zone) had transformed to β and on cooling retransformed to α_2. The α_2 is acicular in nature and distributed throughout the microstructure with distinct prior β grain boundaries already resolvable (marked by the arrows). The coarseness of the α_2 platelets increased with distance from the fusion line. Also, there was considerable grain growth of the prior β grains in the regions close to the FZ. Regions of the HAZ exposed to temperatures below the β transus but in the $\alpha_2 + \beta$ region resulted in a duplex microstructure—Fig. 12. The characteristic feature of this region was equiaxed grains of α_2 with thin β regions-marked by arrows in Fig. 12.

Microhardness

Microhardness traverses across the EB weldments are shown in Fig. 13 for three different welding speeds and heat inputs. The FZ and HAZ regions were much wider for the high-heat input welds than the low-heat input welds. The microhardness averaged 250 DPH in the base metal and increased to an average of 460 DPH in the FZ and HAZ of welds made at 2.1 mm/s (5 in./min). The transition in hardness from low value to high at the base metal/HAZ boundary was sharp. The maximum hardness in the HAZ and FZ was found to be a function of welding speed and thus the heat input and cooling rates. As the welding speed increased and heat input decreased, the maximum hardness dropped to about 390 DPH. The high hardness of the HAZ and FZ in the welds made at 2.1 mm/s is mainly due to the transformation of β to fine, acicular α_2 phase. The presence of such α_2 in the welds made at a low welding speed and thus high heat input, was confirmed earlier as shown in Fig. 9. The decrease in hardness of welds made at high welding speed (and thus low heat input) in excess of 12.5 mm/s (30 in./min) (higher cooling rate), may be related to the retention of larger amounts of metastable β in the microstructure. Similar observations have been made by other investigators for fast cooling laser beam welds (Ref. 11).

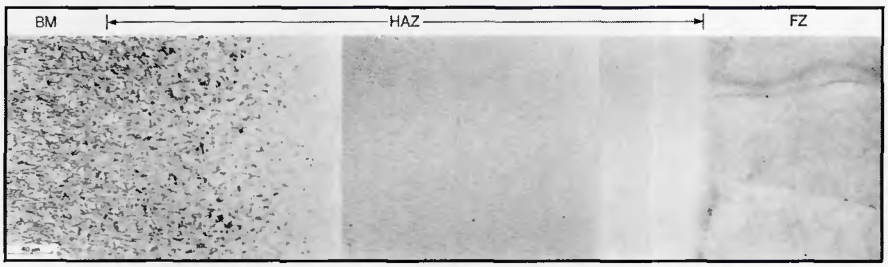

Fig. 12—Photomicrograph showing variations in microstructure across the HAZ of EB weld (welding speed 2.1 mm/s).

Hot Ductility Testing

Hot-ductility tests were performed in a Gleeble 1500 machine that can simulate the rapid heating and cooling of the HAZ in a test specimen. The peak temperature used in the test is below the bulk melting temperature of the alloy investigated. Results of a hot-ductility test may provide significant information on the elevated-temperature tensile properties of any microstructure that may occur within the weld HAZ and hence, the cracking tendency, if any, of the HAZ.

The HAZ weld thermal cycle used for the hot ductility testing was shown earlier in Fig. 5B. Specimens were fractured in tension during both the heating and cooling portions of the thermal cycle. Tensile ductility of the base metal as a function of temperature is shown in Fig. 14. Figure 14B shows the behavior for tests conducted during the heating portion of the HAZ thermal cycle. The ductility of Ti-14-21 alloy increased from 3% at room temperature to 25% at 640°C (1184°F). At higher temperatures, there was a significant amount of scatter in the data, in particular around 800°C (1472°F). Also, the ductility of the specimens tested between 700° to 900°C (1292° to 1652°F) was lower than at 640°C, indicating a ductility "dip" on heating. A ductility dip has been observed in many α/β alloys during the cooling part of a weld thermal cycle and has been reported to be related to the slip and deformation characteristics of the partially transformed β microstructure (Ref. 21). The observed ductility dip in the alloy is a strong function of the cooling rate. In contrast to the earlier studies, in this investigation, a ductility minimum was observed during the heating part of the weld thermal cycle. Since the base metal used in all these tests was in the as-received condition, predominantly consisting of deformed α_2 with a small amount of β (disordered), appreciable phase transformation is not expected in the temperature range 700° to 900°C during the heating part of the thermal cycle. Although no change in the microstructure is expected in this temperature range, the slip mechanism may be different at the temperature of minimum ductility. Further investigation is necessary to confirm this. Also, reasons for the observed scatter in the data are still unresolved. The ductility of specimens

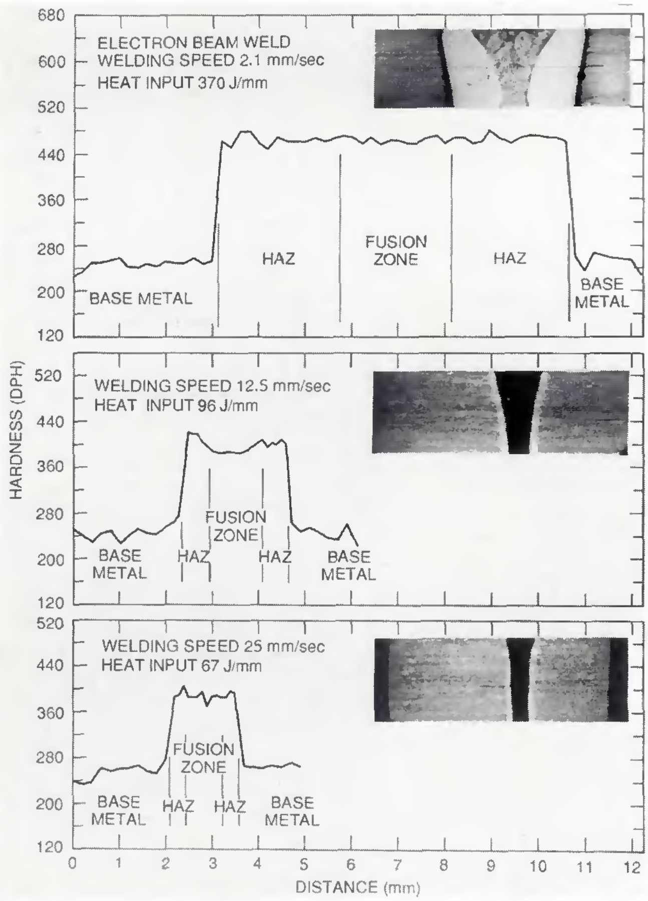

Fig. 13 — DPH microhardness traverse across the transverse sections of three EB weldments made at three welding speeds and heat inputs.

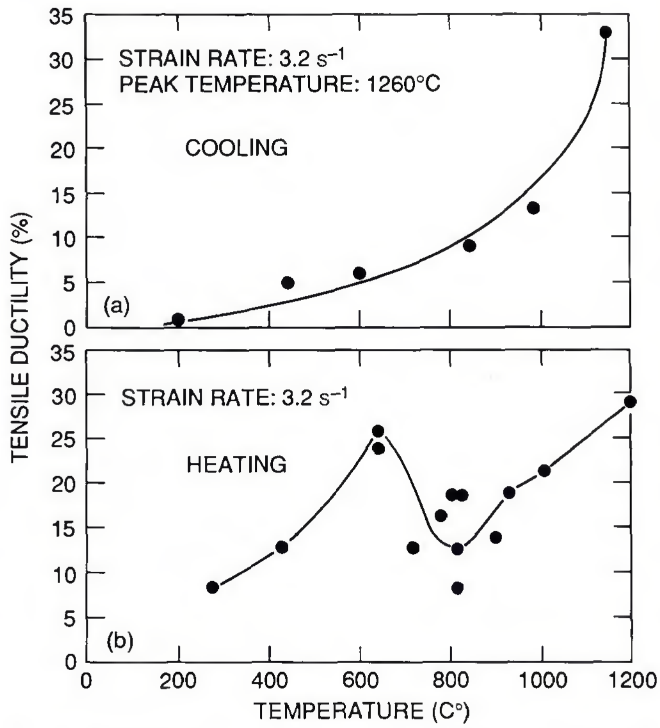

Fig. 14 — Hot ductility response during cooling and heating of Ti-14-21 alloy.

tested at temperatures in excess of 1000°C (1832°F) showed a significant increase. This is related to transformation of α_2 in the base metal to disordered β above 1050°C (1922°F), wherein β is expected to have high ductility.

After reaching a peak temperature of 1260°C (2300°F), the tests conducted during the cooling (Fig. 14A) portion of the Gleeble thermal cycle showed a decrease in ductility from 33% at 1150°C (2102°F) to 0% at 200°C (392°F). At 1000°C and below, the base metal showed significantly lower ductility than the ductility of the alloy during the heating part of the thermal cycle. This is due to the transformation of β (disordered) produced during heating to a temperature above the β transus to mostly brittle acicular α_2 below 1000°C and is undoubtedly related to the anamolous solid-state cracking behavior observed during the Sigmajig testing as noted earlier. The cooling rate encountered during the thermal cycle shown in Fig. 5B is expected to produce a mixture of α_2 with some retained β. This was further confirmed by microstructural analysis. In spite of the loss in ductility during cooling, unlike in some nickel aluminides (Ref. 3), this particular alloy did not exhibit any tendency for HAZ cracking during welding.

Summary

Defect-free EB and GTA welds were produced in the niobium-modified titanium aluminide alloy, Ti-14-21. Weldability evaluation using the Sigmajig test showed excellent resistance of this alloy to hot cracking, as good or better than other weldable aluminides such as Ni_3Al. Although the alloy showed excellent resistance to solidification cracking, it showed a tendency to crack (solid-state cracking) during cooling subsequent to the Sigmajig test. This is attributed to the solid-state transformation of β to a brittle acicular α_2 microstructure during cooling from elevated temperatures. This observed cracking was unique to the highly stressed test specimens only and was not observed in any of the EB or GTA welds produced for evaluation. The hardness of the EB welds varied significantly across the weldment, increasing significantly in the HAZ and FZ. The maximum hardness was found to be influenced by welding speed (heat input), and hence, cooling rate and associated microstructures in the HAZ and FZ.

The microstructural features of the weldments were found to be a strong function of welding speed, heat input, and thus the cooling rate. The FZ microstructures contained predominantly fine, acicular ordered α_2 phase at low welding speeds (that is, high heat input, lower cooling rate), and β and ordered β (B2) phases at high welding speeds (that is, low heat input and high cooling rate). The retention of β at high cooling rates was the primary reason for the decrease in maximum hardness of the FZ at high welding speeds. In the HAZ, there was a gradual variation in microstructures from α_2 acicular near the fusion line to equiaxed $\alpha_2 + \beta$ in the far HAZ.

The Gleeble hot-ductility test revealed an increase in the ductility of the alloy at elevated temperatures, with a possible ductility dip on heating around 830°C. Further, the specimens tested at various temperatures during cooling after reaching a peak temperature above the β transus showed a gradual drop in ductility from 33% at 1150°C to 0% at 200°C with no evidence of a ductility dip. These variations in ductility during the heating or cooling parts of the thermal cycle may be closely related to the complex phase transformations namely $\alpha_2 + \beta$ to β, or β to α_2, respectively.

Acknowledgments

The authors thank C. T. Liu and E. P. George of Oak Ridge National Laboratory, Oak Ridge, Tenn., M. J. Cieslak of Sandia National Lab, Albuquerque, N. Mex., W. A. Baeslack of Ohio State University and T. Kelly of GE Aircraft Engines, Cincinnati, Ohio, for reviewing the manuscript. This research was sponsored by the Div. of Materials Sciences, U.S. Dept. of Energy, under contract DE-AC05-84OR21400 with Martin Marietta Energy Systems, Inc.

References

1. David, S. A., Jemian, W. A., Liu, C. T., and Horton, J. A. 1985. Welding and weldability of nickel-iron aluminides. *Welding Journal* 64(1):225-285.
2. David, S. A., Braski, D. N., and Liu, C. T. 1986. Structure and properties of welded long-range ordered alloys. *Welding Journal* 64(4):93-s to 98-s.
3. Santella, M. L., and David, S. A. 1986. A study of heat-affected zone cracking in Fe-containing Ni_3Al alloy. *Welding Journal* 65(5):129-s to 137-s.
4. Santella, M. L., David, S. A., and Horton, J. A. 1987. Weldability of an Ni_3Al alloy. Advances in Welding Science and Technology, *Proceedings of an International Conference on Trends in Welding Research,* Gatlinburg, Tenn. ASM International, pp 629-633.
5. Santella, M. L., Maguire, M. A., and David, S. A. 1989. Analysis of heat-affected zone cracking in Ni_3Al alloy welds by computer modeling of thermal stresses. *Welding Journal* 68(1):19-s to 27-s.
6. Schechtman, D., Blackburn, M. J., and Lipsitt, H. A. 1974. The plastic deformation of TiAl. *Met. Trans.* 5:1373.
7. Lipsitt, H. A., Schechtman, D., and Schafrik, R. E. 1975. The deformation and fracture of TiAl at elevated temperatures. *Met. Trans. A* 6A: 1991-1996.
8. Lipsitt, H. A. 1985. Titanium aluminides — an overview, high-temperature ordered intermetallilc alloys. *Mat. Res. Soc. Symp. Proc.*, Vol. 39, pp. 351-364.
9. Rhodes, C. G., Hamilton, C. H., and Paton, N. E. 1987. *Titanium Aluminides for Elevated Temperature Applications.* AFML-TR-78-130.
10. Strychor, R., Williams, J. C., and Soffa, W. A. 1988. Phase transformations and modulated microstructures in Ti-Al-Nb alloys. *Met. Trans. A.,* 19A:225.
11. Baeslack, W. A., Cieslak, M. J., and Headley, T. J. 1988. Structure, properties and fracture of pulsed Nd:YAG laser welded Ti-14.8 wt-% Al-21.3 wt-% Nb titanium aluminide. *Scripta Metall.* 22: 1155-1160.
12. Baeslack, W. A., Mascorella, T. J., and Kelly, T. J. Weldability of a Ti_3Al-Nb titanium aluminide. *Welding Journal* 68(12):483-s to 498-s.
13. Goodwin, G. M. 1987. Development of a new hot-cracking test — the Sigmajig. *Welding Journal* 66(2):35-s to 38-s.
14. Vagi, J. J., Meister, R. P., and Randall, M. D. 1968. *Weldment Evaluation Methods,* DMIC 244.
15. Williams, J. C., and Luetjering, G. 1980. The effect of slip length and slip character on the properties of titanium alloys. *Proceedings of the Fourth International Conference on Titanium,* eds. H. Kimura and O. Izmur.
16. Seagle, S. R. 1968. *Principles of Alloying Titanium.* Metals Engineering Institute, ASM, pp. 10-12.
17. Mascorella, T. J. Weldability of Ti_3Al-Nb alloy. M. S. Thesis, Ohio State University, Columbus, Ohio.
18. Nartova, T. T., and Sopochkin, G. G. 1970. Russian Metallurgy. *Metally* 2:138.
19. Andreyev, O. N. 1970. Russian Metallurgy. *Metall.* 2:127.
20. Sastry, S. M. L., and Lipsitt, H. A. 1977. Ordering transformations and mechanical properties of Ti_3Al and Ti_3Al-Nb alloys. *Met. Trans. A,* 8A:1543.
21. Damkroger, B. K., Edwards, G. R., and Rath, B. B. 1989. Investigation of subsolidus weld cracking in alpha-beta titanium alloys. *Welding Journal* 68(7):290-s to 302-s.
22. H. B. Smartt, Idaho National Engineering Laboratory, Idaho Falls, Idaho, private communication, Jan. 1990.
23. T. Mustaleski, Martin Marietta Energy Systems, Inc., Oak Ridge, Tenn., private communication, Jan. 1990.